A SEMI-AUTOMATIC TECHNIQUE FOR GENERATING PARAMETRIC FINITE ELEMENT MODEL OF FEMUR FROM IMAGING MODALITIES

Mehran Armand (1), Thomas J Beck (2), Michael Boyle (1), Maria Z Oden (3), Liming Voo (1), Jay R Shapiro(4)

(1) The Johns Hopkins University Applied Physics Laboratory, Laurel, MD.
(2) Department of Radiology, School of medicine, The Johns Hopkins University, Baltimore, MD.
(3) Department of Orthopedics, University of Texas, Houston, TX.
(4) Department of Medicine, Uniformed Services University of Health Sciences, Bethesda, MD.

INTRODUCTION

Biomechanical phenomena such as aging of the bone, osteoporosis, and bone loss in microgravity affect bone strength by changing its structural geometry. Therefore, the investigation of the individual effects of structural and geometrical parameters on the bone strength can lead to a better understanding of the mechanisms and risk factors associated with a specific bone disease. In this study, we introduce a computational model that allows its parameters to be systematically varied in ways that are observed in aging, spaceflight or with other structural perturbations. The input data to the model can come from Computed Tomography (CT) or APL's newly developed three- dimensional Dual Energy X-Ray Absorptiometry (DEXA) scanner.

Three-dimensional finite element (FE) analysis is the only available technique that accounts for the complexity of the hip geometry and its material distribution. A major challenge for applying FE models is the generation of quality meshes for patient-specific data acquired from imaging modalities. Two common approaches for FE mesh generation are: 1) Direct generation of FE models from CT data (voxel-based methods) [1]. 2) Generation of FE models from the solid / surface models of the femur (the solid or surface model is usually developed by extracting inner and outer contours and reconstructing the surface geometry from the CT scans [2]). The former approach is automated but usually produces unrealistic jagged and non-smooth geometry. The latter approach produces a smooth geometry but is labor intensive. Depending on the application, reasonable accuracy has been reported for both approaches [3]. Because these approaches were mainly created for CT data, they may not be directly applicable to other imaging modalities such as DEXA. Also, since these FE models were not created by parameterization of the femur, they may not directly lend themselves to a sensitivity analysis of the femur's structural and geometrical factors.

The objective of this work was to develop a semi-automatic parametric technique for creating FE models of the femur. The technique can be applied to both CT and DEXA data (a 3D DEXA scanner is currently under development at APL). Similar to the geometry-based techniques, our FE mesh creates a smooth surface geometry. Our approach develops a mechanically-equivalent bone by preserving the cross-sectional mass and moment of inertia of the original geometry.

METHODS

A proximal femur of an average male cadaver was scanned using a CT scanner. Semi-automatic custom algorithms were applied to extract the bone's outer contours and density information from the CT data. An elliptical fit was applied to parameterize the outer contours. The inner contour ellipses were calculated such that the constraint equations for cross-sectional mass and moment of inertia along femoral shaft and neck axes were satisfied. Structural analysis of the bone was performed using I-DEAS software. The following is the three steps required for developing a parametric FE model:

Semi-automatic extraction of the femur geometry and density data

The first step toward the development of a finite element model of the femur was to extract the density maps and bone surface geometry from medical image data (CT scans in this case). We adapted the technique of extracting bone density data from a proximal femur, based on the work of Oden et al. [4].

We scanned a proximal femur of an average male using computed tomography (CT). Our algorithm cropped the CT images to include only the proximal femur. The gray scale and density values were calibrated using a phantom. The horizontal slices were rotated such that the shaft axis was positioned vertically when looking at the longitudinal (vertical) slices of the femur. Next, the algorithm re-sliced images along the axis of the shaft and neck of the femur (the transition from shaft axis to neck axis was defined by a hyperbolic fit). Edge extractions were performed for the outer boundaries of the femur using the re-sliced sections along the femur's neck and shaft axes. The outer boundaries were parameterized by applying non-linear least-square fit of an elliptical equation.

Calculation of the inner boundary of the bone

In order to create a mechanically-equivalent parametric model of the femur, the moment of inertia and the mass of the bone and the model must be equal for each cross-section of the bone. We calculated the cortical/cancellous and cortical/marrow boundary such that the cross-sectional moment of inertia (CSMI) and cross-sectional area (CSA) of the model and the original bone remained equal (note that both are calculated from the mass of the cross-section based on one voxel thickness). We used the density map data for each cross-section plus the CSMI and CSA equations to calculate the appropriate elliptical fit for the cortical/cancellous or cortical/marrow boundaries. This enabled us to define the bone geometry and its material distribution with a finite number of control points for each cross-section. Thus, a full parametric model of the femur was created.

The algorithm accounted for the cortical thickness variations within a cross-section of the bone by allowing eccentric inner contours with respect to their corresponding outer contours. The coordinates of the center of inner ellipses, x_i, was found by manipulating the equations for the first moment of inertia as follows:

$$x_i = \frac{A_o \cdot x_o - CSA \cdot x_{cg}}{A_i}$$

Where x_o is the coordinates of the outer ellipse, x_{cg} is the coordinates of the centorid of the density map, A_o is the area under the outer elliptical ellipse, and A_i is the area under the inner ellipse.

The tissue porosity, μ, for the trabecular volume enclosed by the cortex varies with each cross-section. The value of the trabecular porosity was defined and adjusted for each cross-section using the following equation:

$$\mu = 1 - \frac{\sum_{j=1}^{N} d_j}{N \cdot \rho}$$

Where N is the number of pixels in the inner cortex, d_j is the density value for each pixel, and ρ is the average tissue density from CT.

Automatic generation of the finite element brick mesh

Our programs generated macros for I-DEAS software (also known as program files) that automatically generated 20-node brick elements for the cortical, cancellous, and marrow volumes. The volume inside the inner cortex was then filled with a brick element mesh representing cancellous bone and marrow. The cortical shell included two layers of brick elements. We assumed a modulus of elasticity of 17 GPa for cortical bone and 1.5 GPa for the cancellous bone (the latter can be adjusted to accommodate changing trabecular porosity). Poisson's ratio for bone tissue was taken as 0.33.

SIMULATION EXAMPLES

Defining bone loss in spinal cord injury patients

Progressive bone loss occurs in tetraplegic and paraplegic spinal cord injury (SCI) patients, is not prevented by rehabilitation therapy and is believed to simulate bone loss in space-flight. We modeled the changes in bone structure and stress distribution for the single stance configuration using the data from SCI patients at 0, 6, and 12 months. We demonstrated a progressive increase of the bone maximum stress in SCI patients during the study period. Figure 1 shows a typical finite element simulation of an SCI patient for data collected at 0 and 6 months. Simulation was performed with a distributed pressure of 2 MPa applied to the femoral head, simulating the single stance phase. The simulation showed a 30% increase in the femur's maximum stress (from 13.9 to 19.7 MPa) at the femoral neck due to the loss of bone mass during the 6-month period.

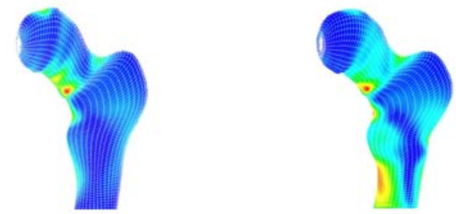

Figure 1: Finite element analysis of the proximal femur of a SCI patient. von Mises stress distribution is calculated from CT A) at 0 month, and B) after 6 months

Effects of geometry on the strength of femoral neck

Figure 2A shows the stress distribution in the proximal femur of a healthy normal male. For this simulation we applied Kinematic constrains to the most distal part of the shaft. A single distributed vertical force of 2500 N was applied to the superior surface of the femoral head. As shown in Figure 2B, we reduced the angle of the neck axis with respect to the longitudinal axis of the shaft by increasing the angle between adjacent planes in the region that included the greater trochanter, with an accumulated total increase of 15 degrees. The simulations showed that with the neck angle reduction, the maximum stress remained at the inferior root of the neck with a 9% reduction in magnitude. However, the stress at the superior root increased by approximately 85% of its original magnitude. Since the fracture strength of bone is significantly lower in tension than compression, this demonstrates a potential mechanism for a transition from compression to tension fractures.

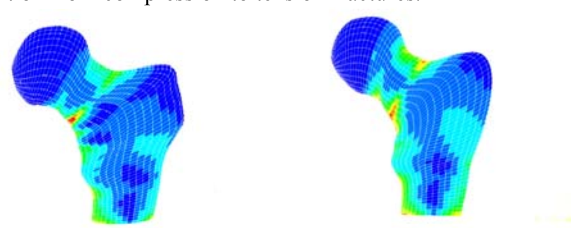

Figure 2: von Mises stress of the proximal femur of A) a healthy male B) when neck angle is changed 15°

REFERENCES

1. Keyak, J. H., Meagher, J.M., Skinner, H.B., and Mote C.D., 1990, "Automated three-dimensional finite element modelling of bone: a new method," *J Biomed Eng*; 12(5):389–397.
2. Lengsfeld, M., Schmitt, J., Alter, P., Kaminsky, J., and Leppek R., 1998, "Comparision of geometry-based and CT voxel-based finite element modeling and experimental validation," *Medical Engineering & Physics* 20: 515-522.
3. Viceconti M, Bellingeri L, Cristofolini L, and Toni A, 1998, "A comparative study on different methods of automatic mesh generation of human femurs," *Medical Engineering and Physics* 20: pp. 1–10.
4. Oden Z.M., Selvitelli D.M., and Bouxsein M.L., 1999, "Effect of local density changes on the failure load of the proximal femur," *J Orthop Res* 17(5):661-667.